

## Supporting information for

# Electrical monitoring of organic crystal phase transition using MoS<sub>2</sub> field effect transistor

**Ilan Boulet<sup>1</sup>, Simon Pascal<sup>1</sup>, Frederic Bedu<sup>1</sup>, Igor Ozerov<sup>1</sup>, Alain Ranguis<sup>1</sup>, Thomas Leoni<sup>1</sup>, Conrad Becker<sup>1</sup>, Laurence Masson<sup>1</sup>, Aleksandar Matkovic<sup>2</sup>, Christian Teichert<sup>2</sup>, Olivier Siri<sup>1</sup>, Claudio Attacalite<sup>1</sup>, Jean-Roch Huntzinger<sup>3</sup>, Matthieu Paillet<sup>3</sup>, Ahmed Zahab<sup>3</sup> and Romain Parret<sup>1\*</sup>**

<sup>1</sup>Aix Marseille Université, CNRS, CINAM, UMR 7325, Campus de Luminy, 13288, Marseille, France

<sup>2</sup>Institute of Physics, Montanuniversität Leoben, 8700, Leoben, Austria

<sup>3</sup>Laboratoire Charles Coulomb, UMR 221, Univ Montpellier, CNRS, Montpellier, France

\*Corresponding author: R.Parret, Aix-Marseille Univ., CNRS, CINAM UMR 7325, 13288 Marseille, France, mobile: +33 (0)6 62922867, , e-mail: romain.parret@univ-amu.fr

### I. Electrical properties

#### a. *In situ* thermal annealing

Prior to any molecular deposition, samples are thermally annealed *in situ* up to 120 °C, in high vacuum (10<sup>-7</sup> mbar) during one hour. Along this step, a drain-source voltage  $V_{DS} = 1$  V is applied to the sample and the drain-source current is measured (Figure S1a). Transfer characteristics  $I_D(V_g)$  in air before pumping and in vacuum after the thermal annealing are presented in Figure S1b. The annealing results in a downshift of the threshold voltage indicating n-type doping. This effect is well documented in the literature and originates from molecular adsorbate removal.<sup>1</sup>

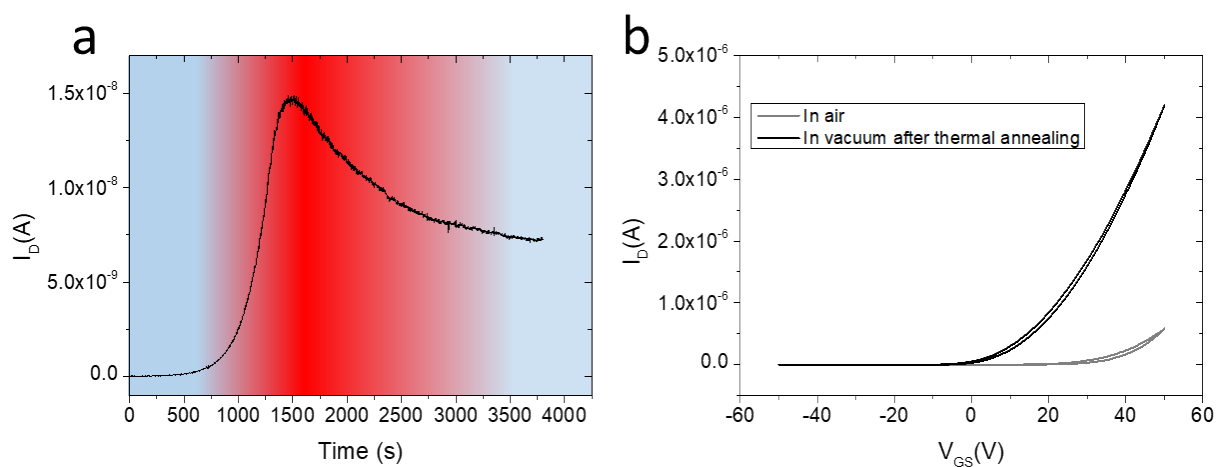


Figure S1 : a. Evolution of the drain-source current *in situ* during the initial thermal annealing carried out by applying  $V_{DS} = 1$  V and  $V_{GS} = 0$  V. Background color illustrates the temperature ramp (blue = room temperature to red = 120°C). b. Transfer characteristics in air before pumping (grey) and in vacuum after the *in situ* thermal annealing (black) ( $V_{DS} = 1$  V).

b. Early stage deposition transfer characteristics

In the experiment presented in this section, we managed to record continuously transfer characteristics during de QZ-C<sub>4</sub> evaporation, *i.e.*, without oven opening as for the data presented in the Figure 2 of the manuscript. The data are presented in the form of a map in Figure S2a. From this map we extract the time dependences of the drain-source current for  $V_{GS}=0V$  and  $V_{GS}=+40V$  (Figure S2b). These results are similar to those presented in the Figure 2, insofar as the two current losses are found around 2000 s and 6000 s and the current increases after QZ-C<sub>4</sub> deposition in comparison to the pristine sample.

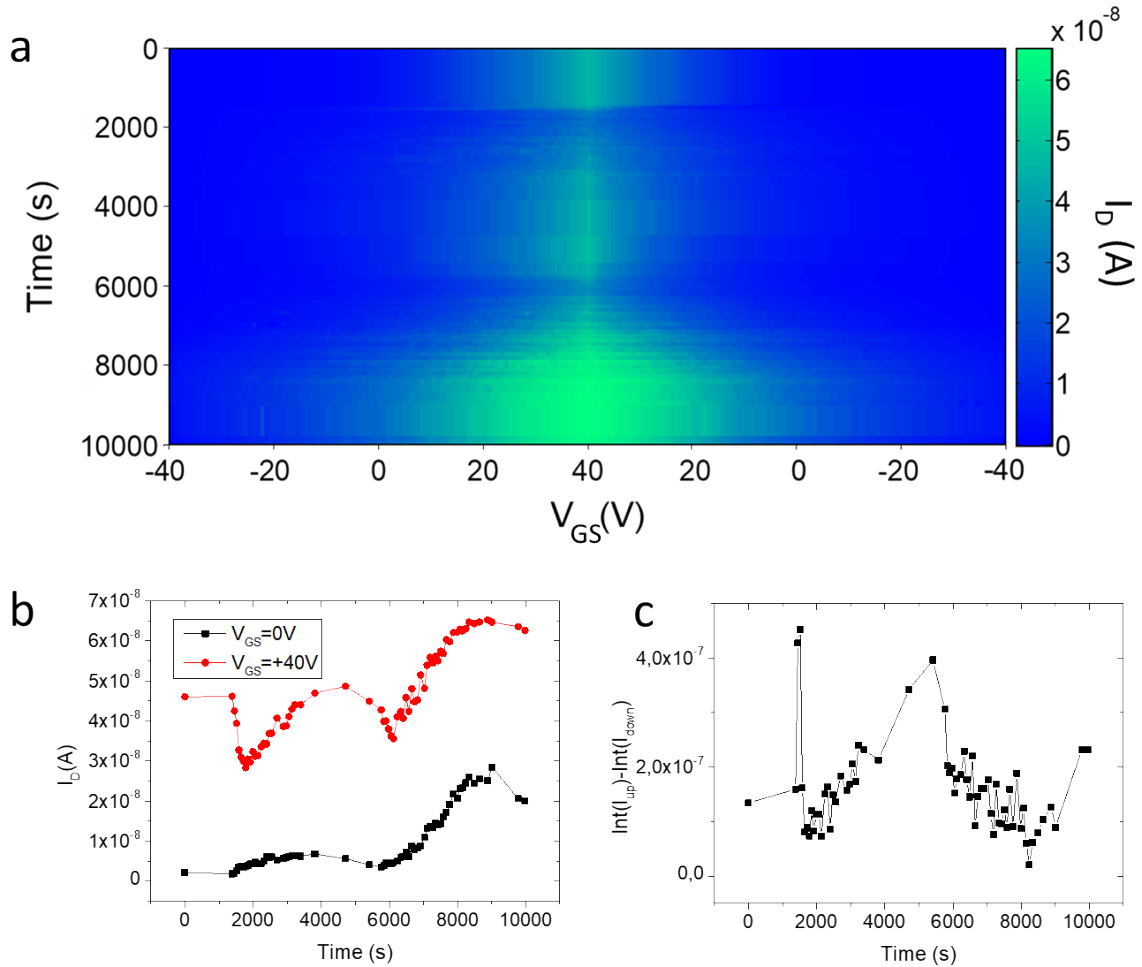


Figure S2: a. Transfer characteristic map of the MoS<sub>2</sub> transistor as a function of the QZ-C<sub>4</sub> deposition time ( $V_{DS} = 1 V$ ). Gate voltage sweeps up are on the left ( $-40 V < V_{GS} < +40 V$ ) and gate voltage sweeps down are on the right ( $+40 V > V_{GS} > -40 V$ ). Evaporation time is on the left axis directed downward and the drain-source current (z-axis) color scale is shown on the right hand side. b. Evolution of the drain-source current as a function of time during evaporation-condensation of the QZ-C<sub>4</sub> for  $V_{DS} = 1 V$ ,  $V_{GS} = 0 V$  (black squares) and  $V_{GS} = +40 V$  (red dots). c. Difference between the areas of the transfer characteristics obtained for increasing  $V_{GS}$  and decreasing  $V_{GS}$  as a function of time.

In Figure S3, we plot the transfer characteristics corresponding to the early stage deposition. The voltage threshold downshifts in a monotonic way with the deposition time. In addition, a hysteresis grows up to a width of 10 V then almost disappears after 1800 s of deposition. In order to highlight the evolution of the hysteresis throughout the evaporation phase, we plot the difference between the areas of the transfer characteristics obtained for increasing  $V_{GS}$  and decreasing  $V_{GS}$  (Figure S2c). This hysteresis cycle is closing downward, similar to what has been observed in QZ/graphene

hybrid transistors.<sup>2</sup> If this had been due to a significant modification of the density of molecules deposited between the rise and fall in gate voltage, we would have observed a cycle closing upwards since the threshold voltage shift induced by the molecules is always oriented towards the negative voltages. This observation indicates that irreversible phenomena, not yet understood, are occurring at almost constant molecular coverage. In Figure S3b, we compare the transfer characteristics of the pristine sample and of the sample after 1980 s of deposition. In addition to the downshift of the threshold voltage, we observe a decrease of the slope in the ON state indicating a diminution of the field effect mobility.

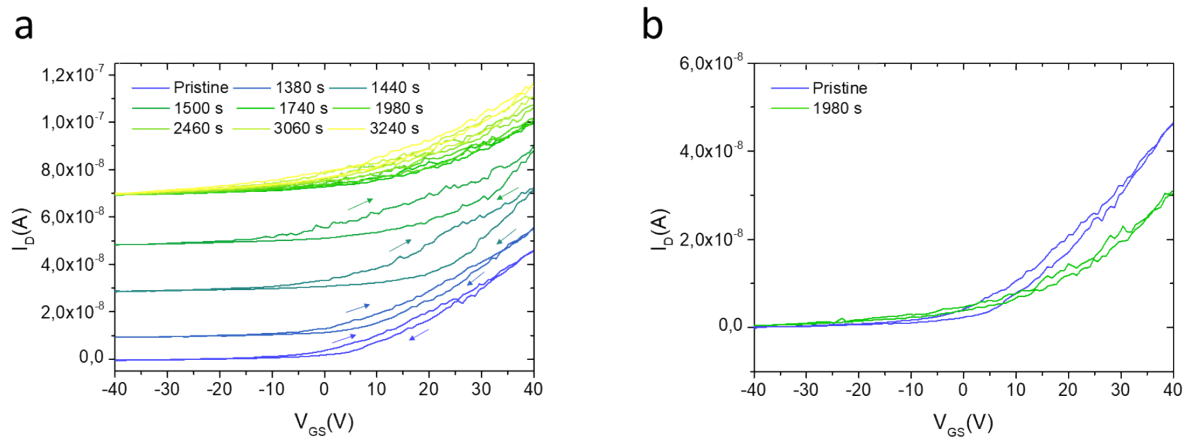


Figure S3: a. Early stage deposition transfer characteristics ( $V_{DS} = 1V$ ). The curves are vertically translated for visibility. Arrows indicate the direction on the gate voltage sweeps. b. Transfer characteristics of the pristine sample (blue) and after 1980 s of deposition (green).

### c. Low temperature thermal annealing

In the manuscript, we present the effect of a thermal annealing of the QZ-C<sub>4</sub> on MoS<sub>2</sub> on the drain-source current. During the temperature profile applied to the sample,  $I_D$  starts by dropping down to a minimum at a temperature in the 70-80 °C range. At this temperature, the sample exhibits an important change visible by eyes due to the evaporation of most of the adsorbed molecules from the MoS<sub>2</sub> surface (Figure S4 a-c). Optical microscopy images allow observing this evolution more precisely. At 70 °C, the elongated crystals begin to degrade (Figure S4 b). At 80 °C, they have completely disappeared leaving a very inhomogeneous phase (Figure S4 c). Concerning the electrical properties, we measured at room temperature the transfer characteristics after thermal annealing realized at 70 °C and 80 °C (Figure S4 d). Both curves exhibit a large hysteresis of about 30 V. We assign such results to a strong disorder induced by the phase transition of the organic crystal.

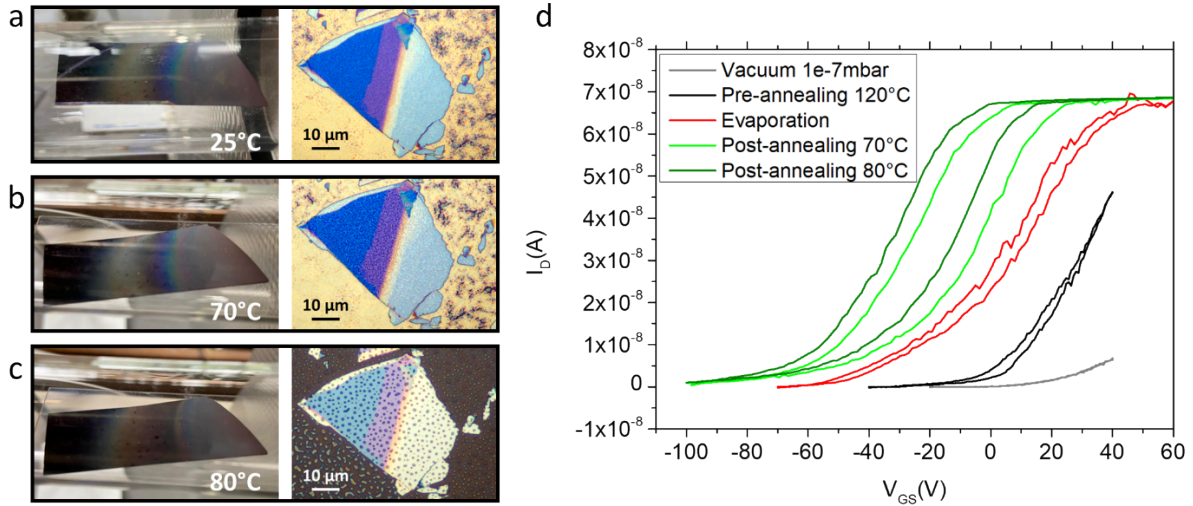


Figure S4: a-c. (Left) Photography of the sample into the evaporator exhibiting a QZ-C<sub>4</sub> gradient concentration at room temperature (a) and after annealing at 70°C (b) and 80°C (c). (Right) optical microscopy images of a selected MoS<sub>2</sub> flake placed at 7 cm from the oven edge at room temperature (a) and after annealing at 70°C (b) and 80°C (c). d. Transfer characteristics of the sample recorded at room temperature before the in situ initial thermal annealing (grey), after the in situ initial thermal annealing (black), after QZ-C<sub>4</sub> deposition (red), after a post-deposition thermal annealing at 70 °C (green), and at 80 °C (dark green).

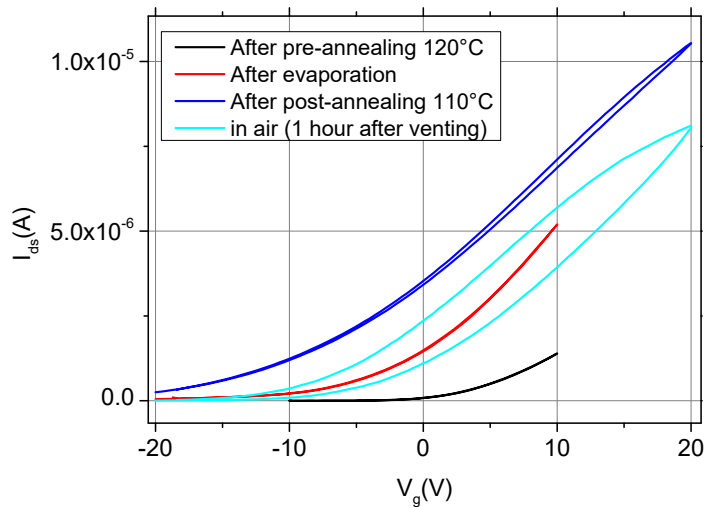


Figure S5: Transfer characteristics of the sample recorded at room temperature after the in situ initial thermal annealing (black), after QZ-C<sub>4</sub> deposition (red), after a post-deposition thermal annealing at 110 °C (blue), and in air one hour after venting

## II. Analysis of the QZ-C<sub>4</sub> morphologies

During the QZ-C<sub>4</sub> deposition, we have shown that at low QZ-C<sub>4</sub> concentration, the molecules form quasi-spherical aggregates (figure 6a-c). Above a critical QZ-C<sub>4</sub> concentration, anisotropic microcrystals are formed (figure 6d-h). During the post-annealing, the majority of the organic layer is re-evaporated leaving a thin organic layer composed of quasi-spherical aggregates, similar to those obtained in the

first stages of the deposition. However, in this annealed phase the aggregates are organized in a highly dense monolayer.

#### a. Determination of QZ-C<sub>4</sub> concentrations

The molecule concentration appears to be a major parameter that determines the conformation that the molecular layer will take. In order to quantitatively verify this hypothesis, we compared, from AFM images, the volume of QZ-C<sub>4</sub> per unit area at different stages of the process.

To carry out this analysis we used the grain module of Gwyddions software by first defining a threshold plane, which corresponds to the surface of the MoS<sub>2</sub>, then, by determining the volume above this threshold and finally by normalizing this volume by the dimensions of the AFM images. The results obtained at the different stages of growth, corresponding to the images of figure 6 of the main manuscript are presented in figure S6 g. The same analysis was carried out for the annealed phase. The concentration obtained (blue line in figure S6 g) close to the critical concentration at which the first crystals appear during the growth. In addition, what really matters is the local concentration, which is much higher during evaporation than during annealing. Indeed, during the evaporation the molecules aggregate together forming increasingly large islands while after annealing the aggregates are organized in a dense monolayer. This implies that locally the QZ-C<sub>4</sub> concentration is much higher during the evaporation than in the annealed phase for which the QZ-C<sub>4</sub> are homogeneously distributed on the surface.

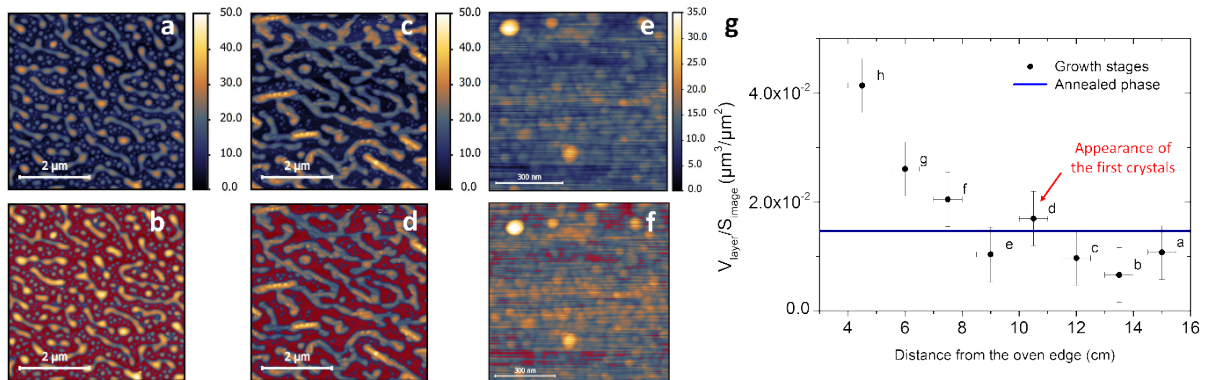


Figure S6: Determination of QZ-C<sub>4</sub> concentrations: AFM images of a growth stage below the critical concentration (a) above the critical concentration (c) and of the annealed phase (e). b,d,f Corresponding images showing the threshold plane. g. Volume of the molecular layer normalized by the AFM image dimensions as a function of the sample distance from the oven edge (symbols). Letters next to the symbols correspond to the AFM image of the figure 6 of the main manuscript. The blue line indicate the QZ-C<sub>4</sub> concentration obtained for the annealed phase.

#### b. Morphologies of the QZ-C<sub>4</sub> layers

In the Figure S7 we present the results of the facet analysis of the as-deposited QZ-C<sub>4</sub> layer.

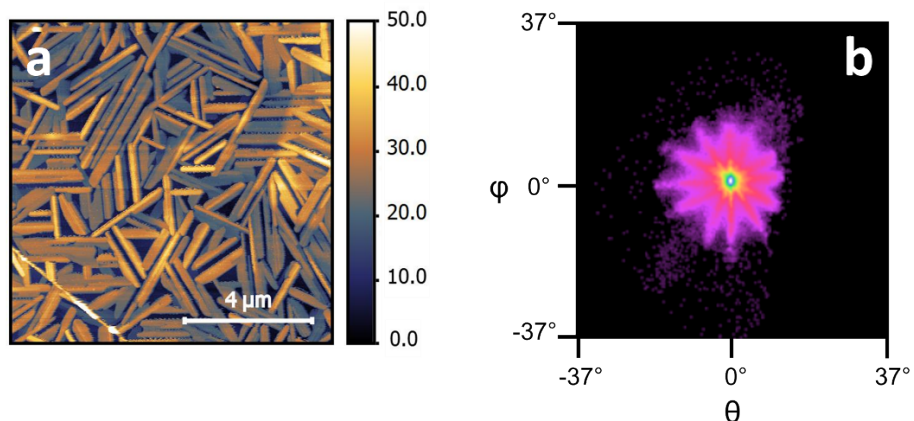


Figure S7: a. AFM image of the the as-deposited QZ-C<sub>4</sub> layer. b. Facet analysis performed on the left image

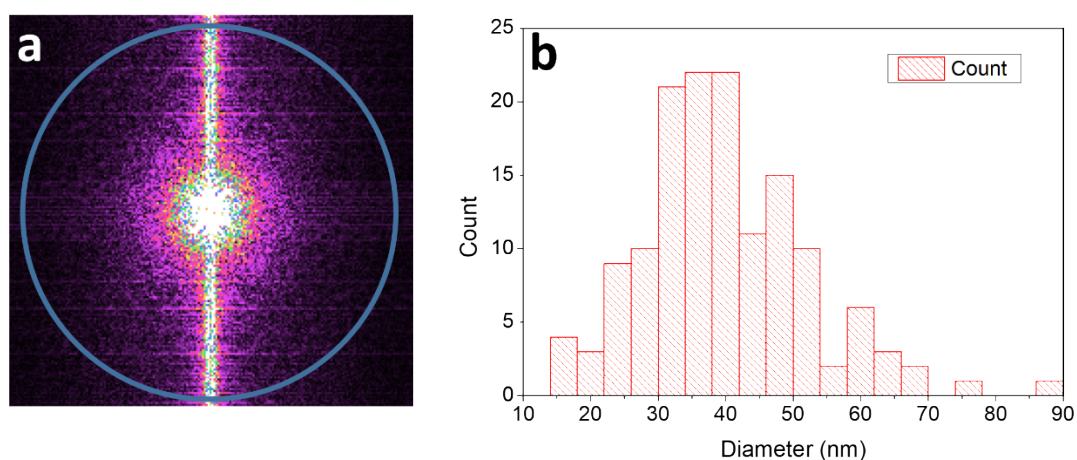


Figure S8: 2D fast Fourier Transform (2D-FFT) of the annealed phase carried out on the AFM image of Figure 3e of the main manuscript. The blue circle is  $0.2 \text{ nm}^{-1}$  in diameter. b. Diameter distribution of the round aggregates also determined from the AFM image of Figure 3e of the main manuscript.

### III. Temperature profile in the molecular doping reactor

We measured the temperature profile in the part of the tube outside the oven for different oven temperatures (Figure S9). All these measurements are recorded under vacuum in stationary operating conditions.

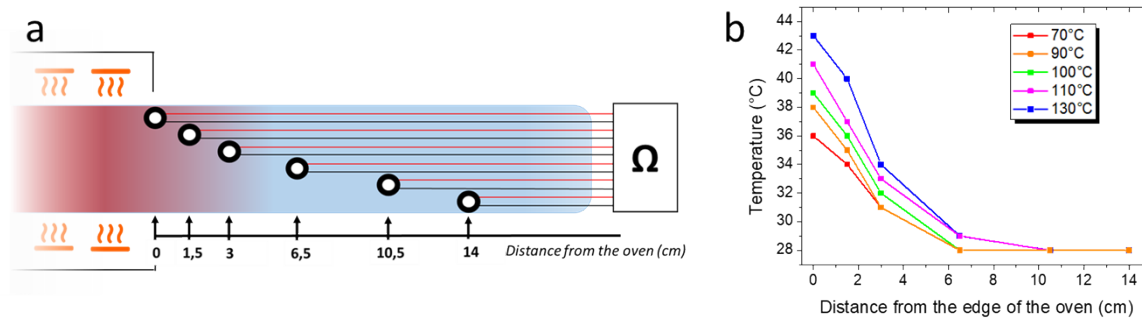


Figure S9: a. Scheme of the molecular doping reactor illustrating the positions of the PT100 probes. b) Temperature profiles in the part of the tube outside the oven for different oven temperatures.

#### IV. DFT calculations: molecular states and binding energies

We consider two cases in the simulation, the case of a single QZ-C<sub>4</sub> molecule deposited on the MoS<sub>2</sub> surface and the case of two molecules in the head to tail configuration. For the first case, we found that two molecular states are present in the MoS<sub>2</sub> band gap (Figure S10). From the DFT results, we obtain also the binding energy of the molecule to the surface. We got 1.28 eV for a single molecule and 1.35 eV for two molecules in head-tail configuration. These two configurations were then used to calculate the charge transfer as described in the main text.

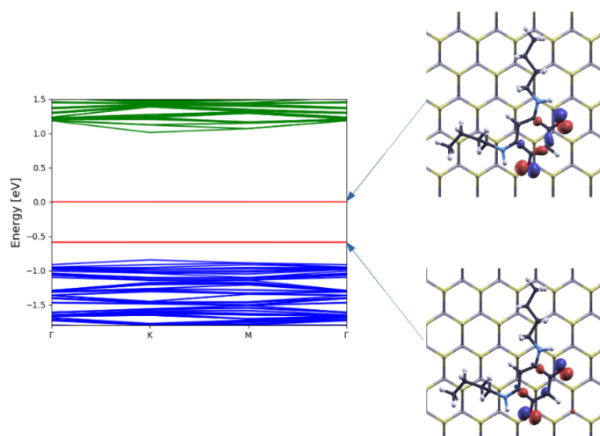


Figure S10: Electronic levels of a single QZ molecule deposited on MoS<sub>2</sub>. Two molecular levels are present in the gap; the corresponding molecular orbitals are shown in the figure.

#### V. Raman spectroscopy

We performed *ex situ* Raman spectroscopy measurements on pristine MoS<sub>2</sub> flakes and after the deposition of QZ-C<sub>4</sub>. An example of the obtained spectra on a MoS<sub>2</sub> monolayer is shown in Figure S11. The main modification concerns the high frequency mode of MoS<sub>2</sub> at a frequency of 400 cm<sup>-1</sup> which is downshifted by 2 cm<sup>-1</sup> and its linewidth increases from 4 cm<sup>-1</sup> to 6 cm<sup>-1</sup>. Such changes are typical signature of induced doping.<sup>3</sup> This confirms that the FET characteristics modifications originate from a channel doping rather than a contact modification.

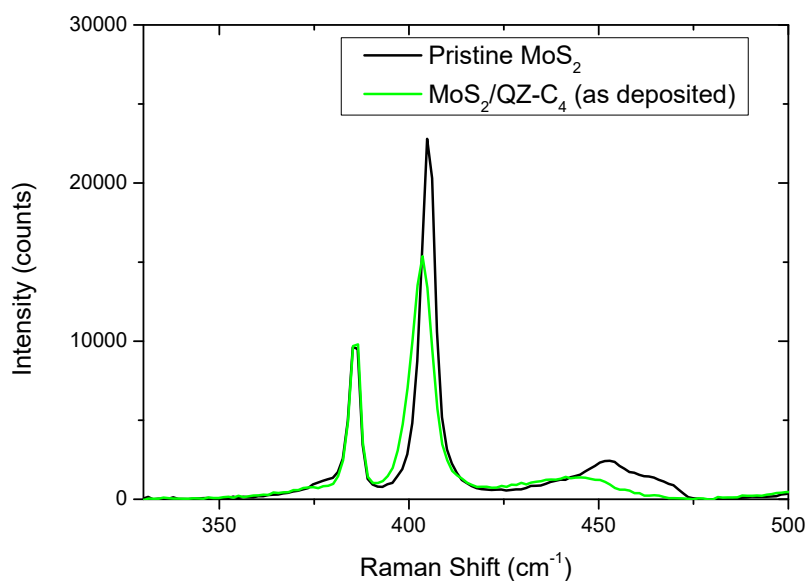


Figure S11: Raman spectra of the same MoS<sub>2</sub> monolayer pristine (black) and after QZ-C<sub>4</sub> deposition (green)

- (1) Krasnozhon, D.; Lembke, D.; Nyffeler, C.; Leblebici, Y.; Kis, A. MoS<sub>2</sub> Transistors Operating at Gigahertz Frequencies. *Nano Lett.* **2014**, *14* (10), 5905–5911. <https://doi.org/10.1021/nl5028638>.
- (2) Mahmood, A.; Yang, C.-S.; Jang, S.; Routaboul, L.; Chang, H.; Ghisolfi, A.; Braunstein, P.; Bernard, L.; Verduci, T.; Dayen, J.-F.; Samorì, P.; Lee, J.-O.; Doudin, B. Tuning Graphene Transistors through *Ad Hoc* Electrostatics Induced by a Nanometer-Thick Molecular Underlayer. *Nanoscale* **2019**, *11* (42), 19705–19712. <https://doi.org/10.1039/C9NR06407A>.
- (3) Chakraborty, B.; Bera, A.; Muthu, D. V. S.; Bhowmick, S.; Waghmare, U. V.; Sood, A. K. Symmetry-Dependent Phonon Renormalization in Monolayer MoS<sub>2</sub> Transistor. *Phys. Rev. B* **2012**, *85* (16), 161403. <https://doi.org/10.1103/PhysRevB.85.161403>.